# Supplementary Information

# Tailoring the d-band center enables La doped $ZnIn_2S_4$ to be active for boosting photocatalytic activation of oxygen and degradation of antibiotic wastewater

Yiwen Hu [a], Xiao Ma [a], Guoli Fan [a*], Lan Yang [a], Feng Li [a,b,*]

[a] State Key Laboratory of Chemical Resource Engineering, Beijing University of Chemical Technology, Box 98, Beijing 100029, China

[b] Beijing Advanced Innovation Center for Soft Matter Science and Engineering, Beijing University of Chemical Technology, Box 98, Beijing 100029, China

* To whom all correspondence should be addressed

Tel.: 8610-64451226; Fax: 8610-64425385.

E-mail: fangl@mail.buct.edu.cn (G.L. Fan);

Lifeng@mail.buct.edu.cn (F. Li)

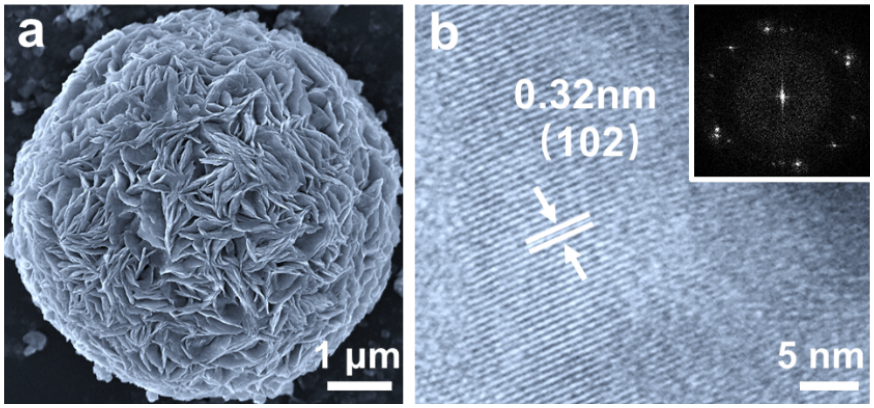


**Fig. S1** (a) FE-SEM image and (b) HRTEM image of ZIS.

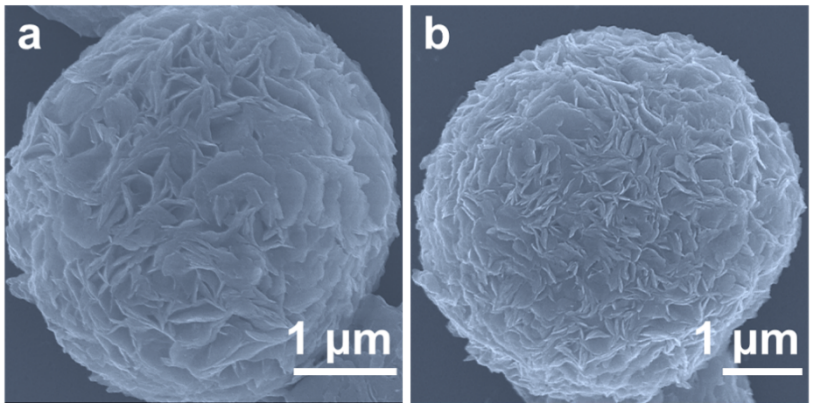


**Fig. S2** FE-SEM image of (a) $La_{1.12}$-ZIS and (b) $La_{1.96}$-ZIS.

**Table S1.** The weight percentage content of elements calculated from ICP-AES and atomic ratio of Zn : In in samples.

| Samples | Zn (wt%) | In (wt%) | La (wt%) | Atomic ratio (Zn:In) |
|---|---|---|---|---|
| $La_{1.12}$-ZIS | 11.88 | 36.79 | 1.12 | 0.3229 |
| $La_{1.37}$-ZIS | 11.45 | 36.23 | 1.37 | 0.3160 |
| $La_{1.96}$-ZIS | 10.77 | 36.58 | 1.96 | 0.2944 |

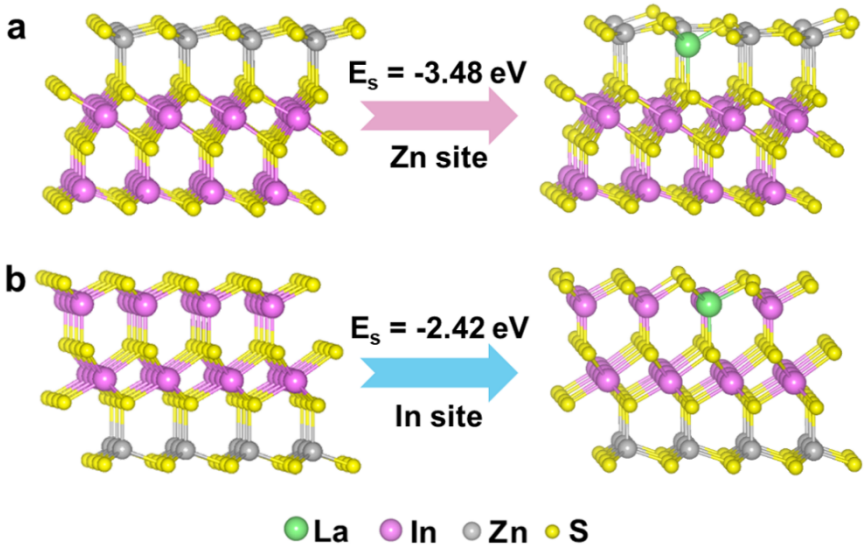


**Fig. S3** The formation energy of La atom for substitution of (a) Zn and (b) In sites.

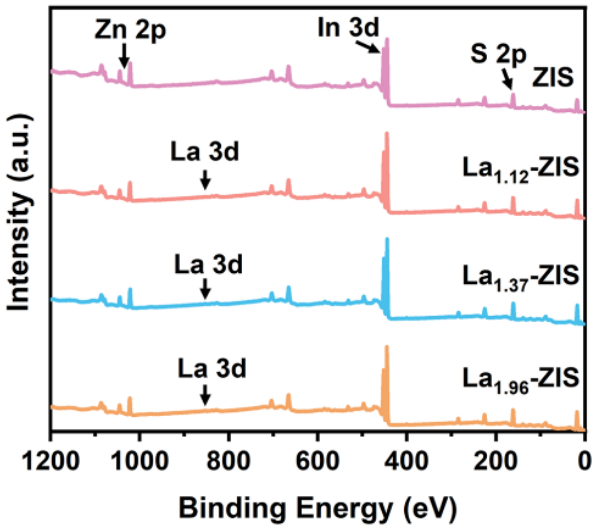


**Fig. S4** XPS survey spectra of ZIS and $La_x$-ZIS.

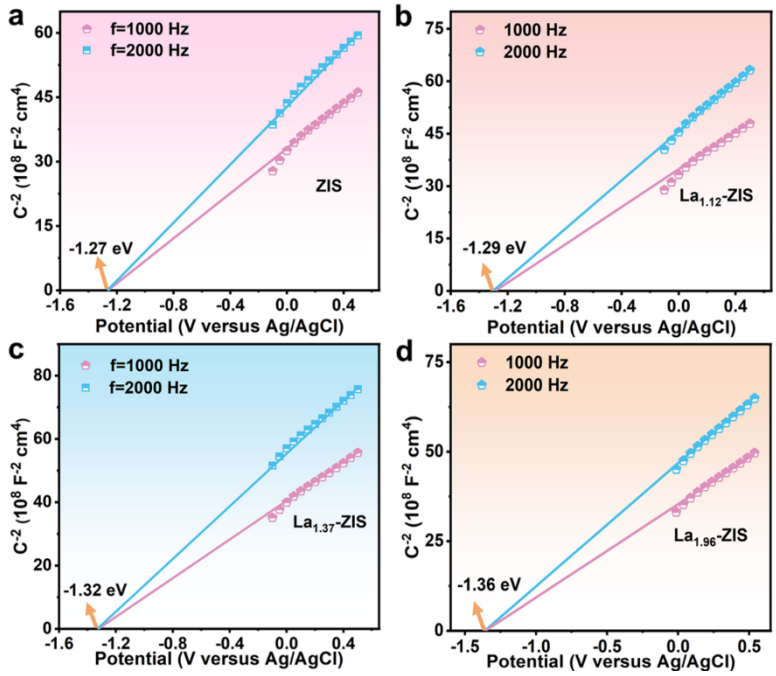


**Fig. S5** Mott-Schottky plots of (a) ZIS, (b) $La_{1.12}$-ZIS, (c) $La_{1.37}$-ZIS and (d) $La_{1.96}$-ZIS.

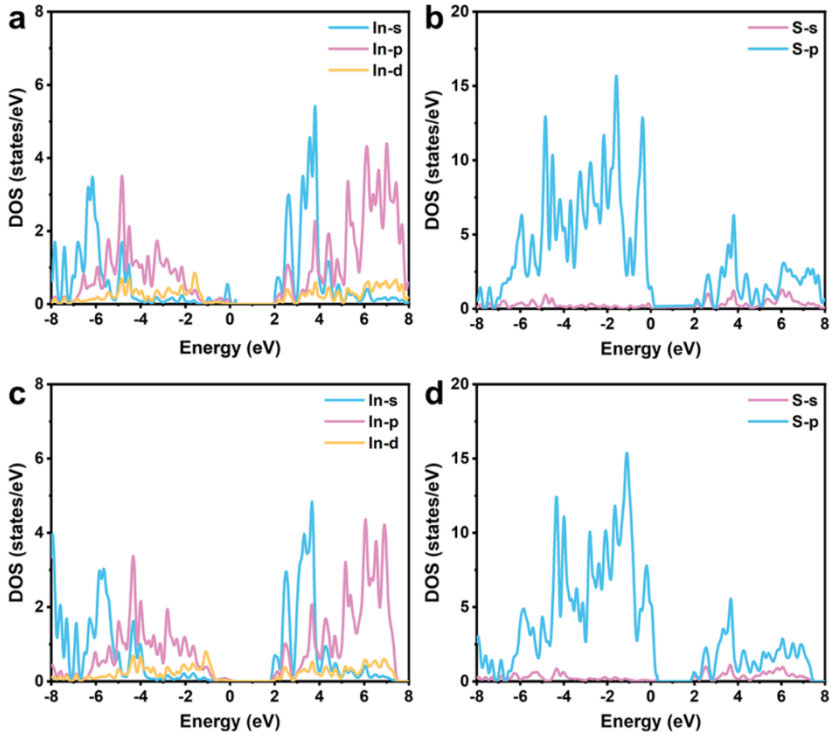


**Fig. S6** Calculated projected density of states of (a-b) ZIS and (c-d) $La_{1.37}$-ZIS.

**Table S2.** Kinetic parameters for the degradation of MNZ determined using pseudo-first-order model.

| Samples | Pseudo-first-order kinetic | |
|---|---|---|
| | K ($min^{-1}$) | $R^2$ |
| ZIS | 0.0144 | 0.9909 |
| $La_{1.12}$-ZIS | 0.0286 | 0.9940 |
| $La_{1.37}$-ZIS | 0.0496 | 0.9877 |
| $La_{1.96}$-ZIS | 0.0206 | 0.9944 |

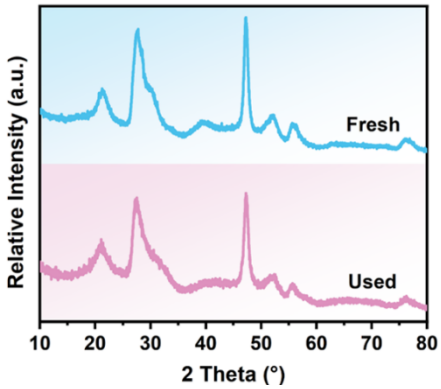


**Fig. S7** XRD patterns of $La_{1.37}$-ZIS before and after cycling experiments.

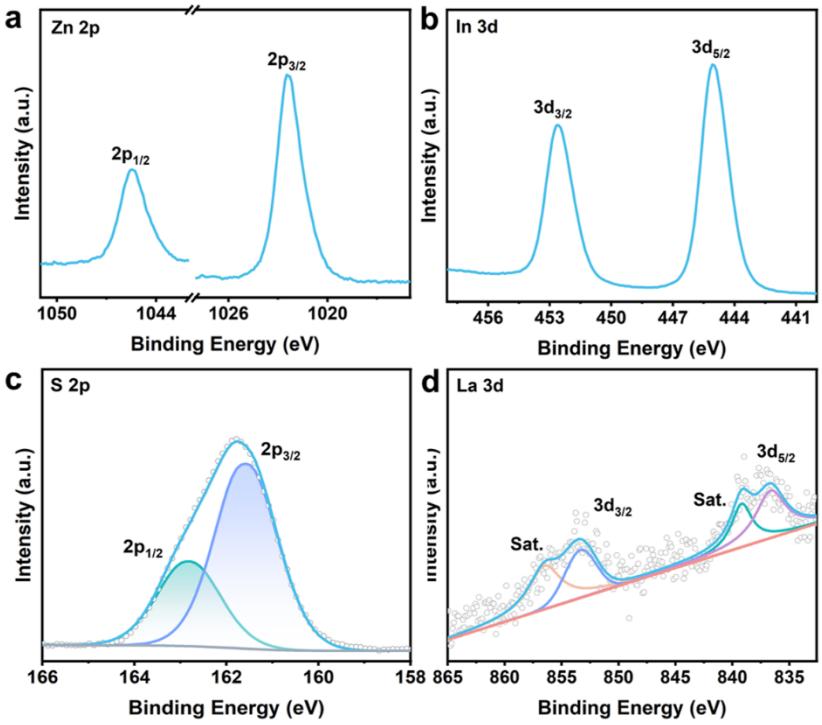


**Fig. S8** (a) Zn 2p, (b) In 3d, (c) S 2p and (d) La 3d XPS spectra of $La_{1.37}$-ZIS after cycling experiments.

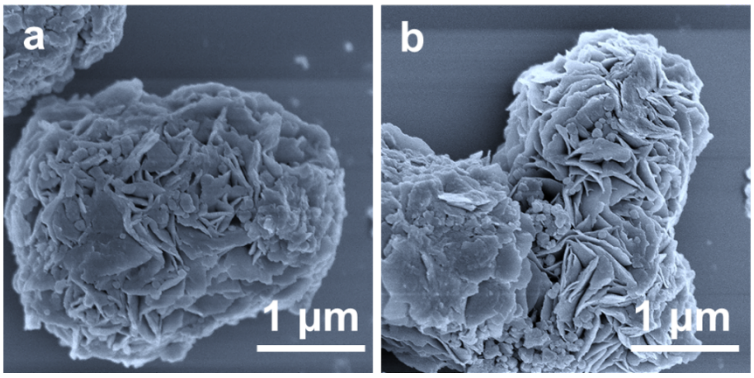


**Fig. S9** SEM images of $La_{1.37}$-ZIS after cycling experiments.

**Table S3.** Kinetic parameters for the degradation of TCH determined using pseudo-first-order and pseudo-second-order model.

| Samples | Pseudo-first-order kinetic | | Pseudo-second-order kinetic | |
|---|---|---|---|---|
| | $K_1$ ($min^{-1}$) | $R_1^2$ | $K_2$ ($L \cdot mg^{-1} \cdot min^{-1}$) | $R_2^2$ |
| P25 | 0.0072 | 0.9688 | 0.0033 | 0.9696 |
| ZIS | 0.0214 | 0.9823 | 0.0186 | 0.9925 |
| $La_{1.12}$-ZIS | 0.0305 | 0.9597 | 0.0382 | 0.9852 |
| $La_{1.37}$-ZIS | 0.0395 | 0.9403 | 0.0643 | 0.9836 |
| $La_{1.96}$-ZIS | 0.0294 | 0.9757 | 0.0326 | 0.9944 |

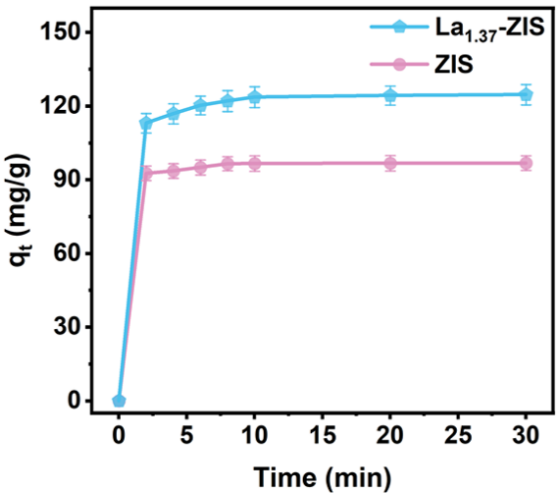


**Fig. S10** The adsorption-desorption equilibrium curves of TCH over ZIS and $La_{1.37}$-ZIS.

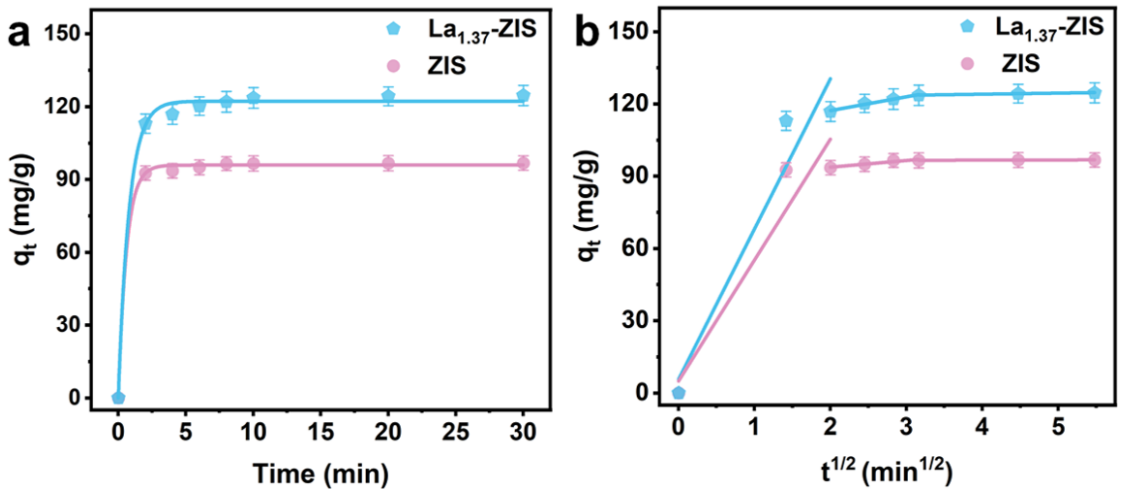


**Fig. S11** (a) The kinetics curves of pseudo-first-order model, (b) intra-particle model for TCH adsorption over ZIS and $La_{1.37}$-ZIS.

**Table S4.** Kinetic parameters for adsorption of TCH over ZIS and $La_{1.37}$-ZIS.

| Kinetic model | Parameter | ZIS | $La_{1.37}$-ZIS |
|---|---|---|---|
| Pseudo-first-order | $K_1$ ($min^{-1}$) | 1.6659 | 1.2542 |
| | $q_e$ ($mg \cdot g^{-1}$) | 95.94 | 122.27 |
| | $R^2$ | 0.9988 | 0.9967 |
| Pseudo-second-order | $K_2$ ($mg \cdot min^{-1} \cdot g^{-1}$) | 0.0951 | 0.0335 |
| | $q_e$ ($mg \cdot g^{-1}$) | 97.21 | 125.61 |
| | $R^2$ | 0.9997 | 0.9996 |
| Intraparticle diffusion | $K_{1dif}$ ($mg \cdot g^{-1}$) | 50.26 | 62.44 |
| | $C_1$ ($mg \cdot g^{-1} min^{-1}$) | 4.8917 | 5.6169 |
| | $R_1^2$ | 0.8470 | 0.8679 |
| | $K_{2dif}$ ($mg \cdot g^{-1}$) | 2.7772 | 5.7261 |
| | $C_2$ ($mg \cdot g^{-1} \cdot min^{-1}$) | 88.20 | 105.80 |
| | $R_2^2$ | 0.9006 | 0.9763 |
| | $K_{3dif}$ ($mg \cdot g^{-1}$) | 0.0702 | 0.4449 |
| | $C_3$ ($mg \cdot g^{-1} \cdot min^{-1}$) | 96.41 | 122.29 |
| | $R_3^2$ | 0.9170 | 0.9740 |

**Table S5.** Comparison of photocatalytic performance of recent reported photocatalysts for the

degradation of MNZ or TCH.

| Samples | Light sources | Pollutant | Degradation efficiencies | Concentration ($mg \cdot L^{-1}$) | Dosage ($g \cdot L^{-1}$) | Refs. |
|---|---|---|---|---|---|---|
| ZnO | Ultraviolet light | MNZ | 63.00% (30min) | 10 | 0.3 | 1 |
| ZnO/PiC | Visible light (λ＞420nm) | MNZ | 97.50% (40min) | 10 | 0.2 | 2 |
| P-doped $g_3N_4/Co_3O_4$ | Visible light (λ＞420nm) | MNZ | 68.90% (180min) | 10 | 1.0 | 3 |
| $Zn_3In_2S_6$/AgBr | Visible light (λ＞420nm) | MNZ | 98.20% (120min) | 10 | 0.5 | 4 |
| B-$TiO_2$/$BiVO_4$ | Visible light (λ＞420nm) | TCH | 89.30 % (120 min) | 20 | 0.5 | 5 |
| Ce-$CdIn_2S_4$ | Visible light (λ＞420nm) | TCH | 85.60 % (120 min) | 50 | 0.5 | 6 |
| $Ag_2O/ZnIn_2S_4$ | Visible light (λ＞420nm) | TCH | 83.66% (100 min) | 10 | 0.35 | 7 |
| $SnS_2$@$ZnIn_2S_4$ @kaolinite | Visible light (λ＞420nm) | TCH | 88.23% (60min) | 40 | 0.2 | 8 |
| $La_{1.37}$-ZIS | Visible light (λ＞420nm) | MNZ | 97.20% (80min) | 60 | 0.33 | This work |
| $La_{1.37}$-ZIS | Visible light (λ＞420nm) | TCH | 87.60% (40min) | 80 | 0.33 | This work |

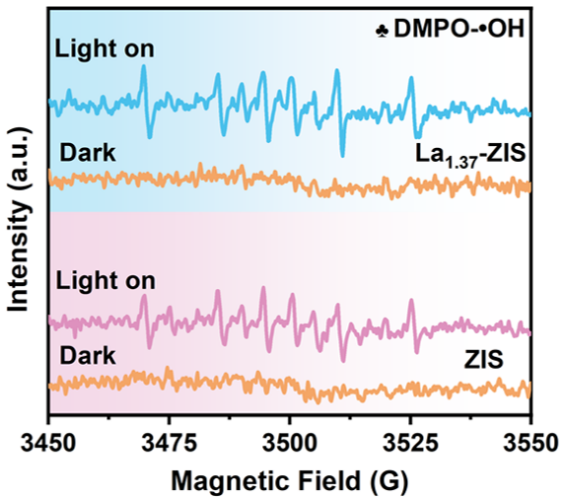


**Fig. S12** DMPO-·OH generated by ZIS and $La_{1.37}$-ZIS in the dark and under visible light

irradiation.

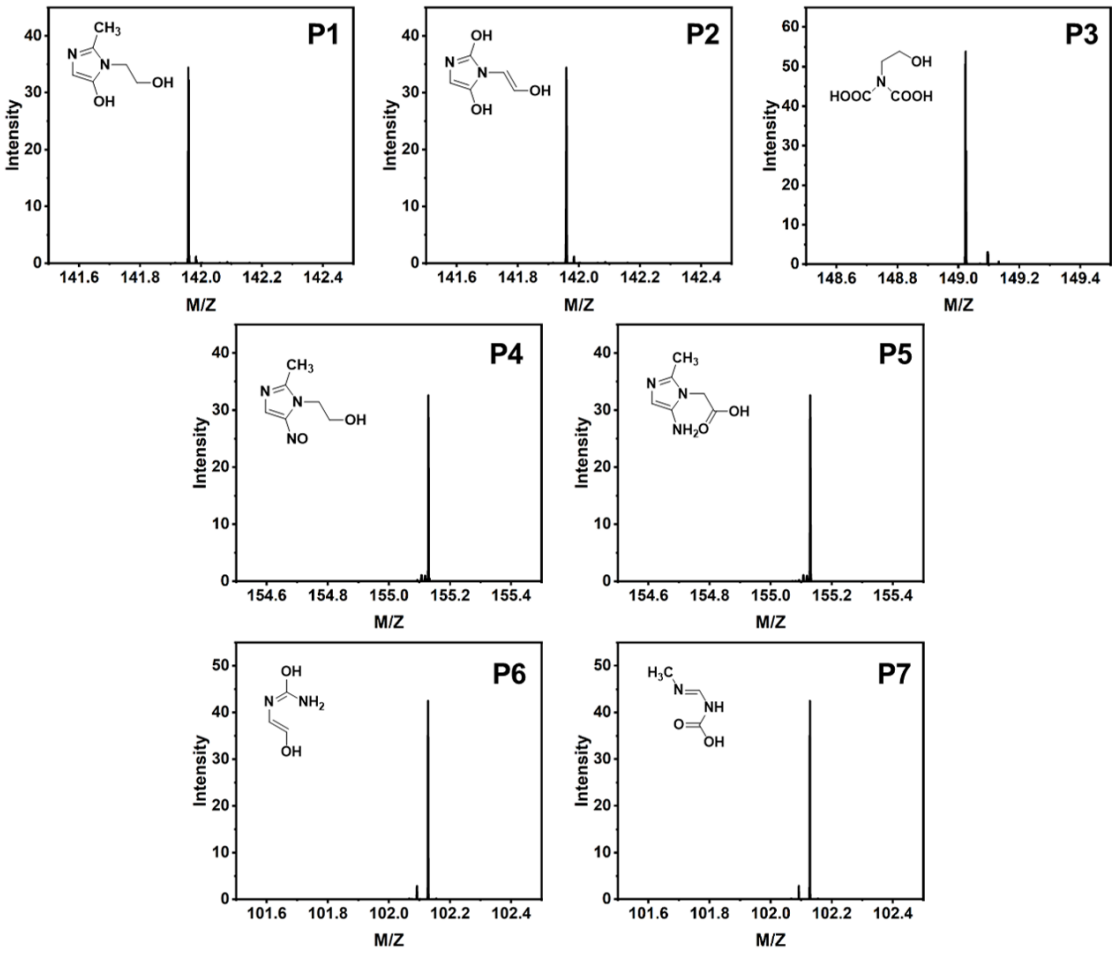


**Fig. S13** Possible intermediates in the photocatalytic degradation of MNZ by $La_{1.37}$-ZIS.

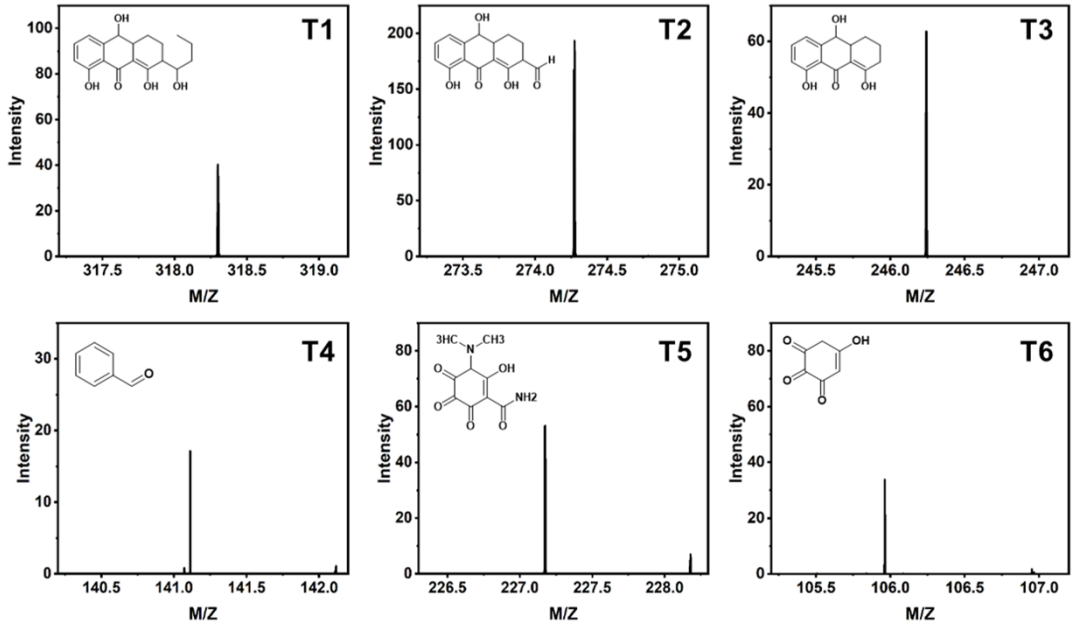


**Fig. S14** Possible intermediates in the photocatalytic degradation of TCH by $La_{1.37}$-ZIS.

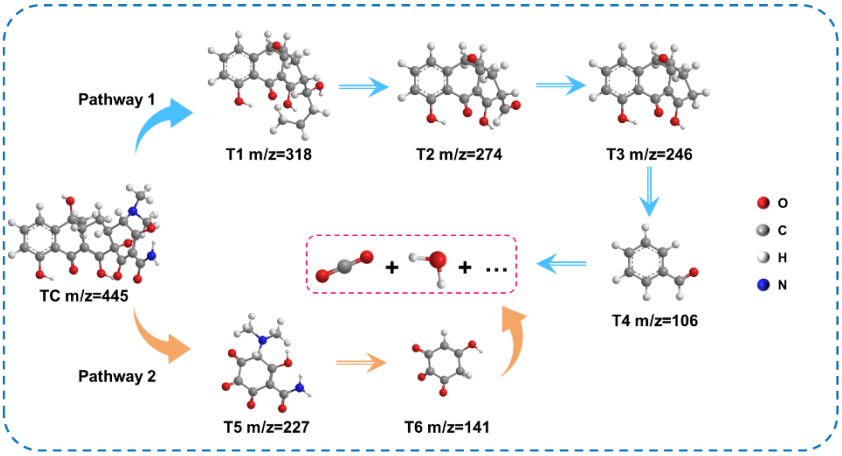


**Fig. S15** Proposed photocatalytic degradation pathways of TCH over $La_{1.37}$-ZIS.

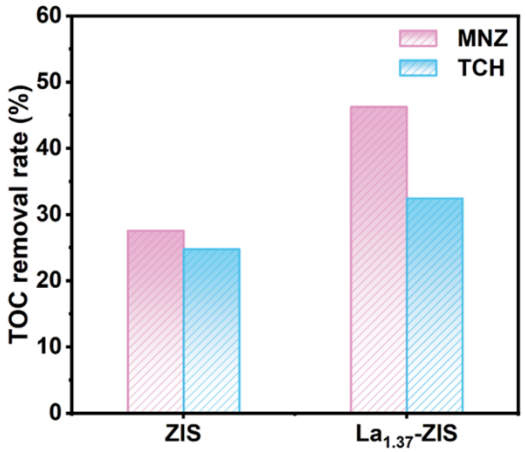


**Fig. S16** TOC removal rate of MNZ and TCH by ZIS and $La_{1.37}$-ZIS.

## Supplementary References


1. M. L. Tran, C.-C. Fu and R.-S. Juang, Removal of metronidazole by $TiO_2$ and ZnO photocatalysis: a comprehensive comparison of process optimization and transformation products, *Environ. Sci. Pollut. Res.*, 2018, **25**, 28285-28295.
2. H. Cai, D. Zhang, X. Ma and Z. Ma, A novel ZnO/biochar composite catalysts for visible light degradation of metronidazole, *Sep. Purif. Technol.*, 2022, **288**, 120633.
3. Z. Zhao, J. Fan, X. Deng and J. Liu, One-step synthesis of phosphorus-doped g-$C_3N_4$/$Co_3O_4$ quantum dots from vitamin B12 with enhanced visible-light photocatalytic activity for metronidazole degradation, *Chem. Eng. J.*, 2019, **360**, 1517-1529.
4. J. Sun, Y. Hou, Z. Yu, L. Tu, Y. Yan, S. Qin, S. Chen, D. Lan, H. Zhu and S. Wang, Visible-light-driven Z-scheme $Zn_3In_2S_6$/AgBr photocatalyst for boosting simultaneous Cr (VI) reduction and metronidazole

oxidation: Kinetics, degradation pathways and mechanism, *J. Hazard. Mater.*, 2021, **419**, 126543.

5. C. Wu, J. Dai, J. Ma, T. Zhang, L. Qiang and J. Xue, Mechanistic study of B-$TiO_2$/$BiVO_4$ S-scheme heterojunction photocatalyst for tetracycline hydrochloride removal and $H_2$ production, *Sep. Purif. Technol.*, 2023, **312**, 123398.
6. F. Wang, W. Zhang, H. Liu, R. Cao and M. Chen, Roles of $CeO_2$ in preparing Ce-doped $CdIn_2S_4$ with boosted photocatalytic degradation performance for methyl orange and tetracycline hydrochloride, *Chemosphere*, 2023, **338**, 139574.
7. Y. Xiao, Z. Peng, W. Zhang, Y. Jiang and L. Ni, Self-assembly of $Ag_2O$ quantum dots on the surface of $ZnIn_2S_4$ nanosheets to fabricate p-n heterojunctions with wonderful bifunctional photocatalytic performance, *Appl. Surf. Sci.*, 2019, **494**, 519-531.
8. Y. Li, B. Yu, Z. Hu and H. Wang, Construction of direct Z-scheme $SnS_2$@$ZnIn_2S_4$@kaolinite heterostructure photocatalyst for efficient photocatalytic degradation of tetracycline hydrochloride, *Chem. Eng. J.*, 2022, **429**, 132105.